



Evaluation of Texture Analysis for the Differential Diagnosis of Mass-Forming Pancreatitis From Pancreatic Ductal Adenocarcinoma on Contrast-Enhanced CT Images

Shuai Ren^{1†}, Jingjing Zhang¹, Jingya Chen¹, Wenjing Cui¹, Rui Zhao¹, Wenli Qiu¹, Shaofeng Duan², Rong Chen³, Xiao Chen¹ and Zhongqiu Wang^{1*†}

¹ Department of Radiology, Affiliated Hospital of Nanjing University of Chinese Medicine, Jiangsu Province Hospital of Chinese Medicine, Nanjing, China, ² GE Healthcare China, Shanghai, China, ³ Department of Diagnostic Radiology and Nuclear Medicine, University of Maryland School of Medicine, Baltimore, MD, United States

OPEN ACCESS

Edited by:

Bo Gao,
Affiliated Hospital of Guizhou Medical
University, China

Reviewed by:

Atsushi Kanno,
Tohoku University, Japan
Xiaofeng Tao,
Shanghai Jiao Tong University, China

*Correspondence:

Zhongqiu Wang
zhqwang001@126.com

†ORCID:

Shuai Ren
orcid.org/0000-0003-4902-6298
Zhongqiu Wang
orcid.org/0000-0001-6681-7345

Specialty section:

This article was submitted to
Cancer Imaging and Image-directed
Interventions,
a section of the journal
Frontiers in Oncology

Received: 02 August 2019

Accepted: 18 October 2019

Published: 05 November 2019

Citation:

Ren S, Zhang J, Chen J, Cui W,
Zhao R, Qiu W, Duan S, Chen R,
Chen X and Wang Z (2019) Evaluation
of Texture Analysis for the Differential
Diagnosis of Mass-Forming
Pancreatitis From Pancreatic Ductal
Adenocarcinoma on
Contrast-Enhanced CT Images.
Front. Oncol. 9:1171.
doi: 10.3389/fonc.2019.01171

Purpose: To investigate the potential of computed tomography (CT) imaging features and texture analysis to differentiate between mass-forming pancreatitis (MFP) and pancreatic ductal adenocarcinoma (PDAC).

Materials and Methods: Thirty patients with pathologically proved MFP and 79 patients with PDAC were included in this study. Clinical data and CT imaging features of the two lesions were evaluated. Texture features were extracted from arterial and portal phase CT images using commercially available software (AnalysisKit). Multivariate logistic regression analyses were used to identify relevant CT imaging and texture parameters to discriminate MFP from PDAC. Receiver operating characteristic curves were performed to determine the diagnostic performance of predictions.

Results: MFP showed a larger size compared to PDAC ($p = 0.009$). Cystic degeneration, pancreatic ductal dilatation, vascular invasion, and pancreatic sinistral portal hypertension were more frequent and duct penetrating sign was less frequent in PDAC compared to MFP. Arterial CT attenuation, arterial, and portal enhancement ratios of MFP were higher than PDAC ($p < 0.05$). In multivariate analysis, arterial CT attenuation and pancreatic duct penetrating sign were independent predictors. Texture features in arterial phase including SurfaceArea, Percentile40, InverseDifferenceMoment_angle90_offset4, LongRunEmphasis_angle45_offset4, and uniformity were independent predictors. Texture features in portal phase including LongRunEmphasis_angle135_offset7, VoxelValueSum, LongRunEmphasis_angle135_offset4, and GLCMEntropy_angle45_offset1 were independent predictors. Areas under the curve of imaging feature-based, texture feature-based in arterial and portal phases, and the combined models were 0.84, 0.96, 0.93, and 0.98, respectively.

Conclusions: CT texture analysis demonstrates great potential to differentiate MFP from PDAC.

Keywords: pancreatic ductal adenocarcinoma, chronic pancreatitis, computed tomography, texture analysis, machine learning

INTRODUCTION

Pancreatic ductal adenocarcinoma (PDAC) is a deadly disease with a grim overall prognosis; its mortality is almost equal to its morbidity (1). The 5-year survival rate for PDAC patients was 7.8% between 2006 and 2012, compared to a 66.9% 5-year survival rate for cancers at all sites (2). Surgical resection is regarded as the only curative treatment option, but most patients are asymptomatic and diagnosed at an advanced stage when the optimal time for surgical resection has passed (1). Therefore, effective and non-invasive screening methods to detect PDAC at an early stage are of utmost importance. This may help to increase the survival rate by providing a chance for early surgical treatment and adjuvant intervention (3, 4).

Mass-forming pancreatitis (MFP) encompasses a gradual form of the ordinary chronic pancreatitis or a specific etiology such as focal type of autoimmune pancreatitis (5, 6), which must be differentiated accurately from PDAC due to their similar presentations of abdominal pain, weight loss, pancreatic insufficiency, and overlapping radiologic features (7–11). Resectional surgery is radical for MFP and may result in pancreatic insufficiency. On the other hand, drainage operations are ineffective for PDAC. The incidence of PDAC in the MFP population is estimated to be 1–6% (12–15). An estimated 5–10% of patients who undergo pancreaticoduodenectomy for suspected pancreatic malignancy are found to have benign lesions on surgical pathologic examination (12, 13). Thus, accurate preoperative differentiation between MFP and PDAC is clinically important for deciding whether or not to perform resection (12). With the application of endoscopic ultrasound fine-needle aspiration biopsy (EUS-FNA), cytopathological evidence can be acquired accurately from pancreatic masses with a reported

sensitivity of 79–98%, specificity of 71–100%, and accuracy of 82–98% (5, 16, 17). However, even EUS-guided biopsies show false negative diagnosis of 12–14%, which may result in delayed patient care (5). Therefore, non-invasive imaging is crucial in the differential diagnosis and treatment strategy planning.

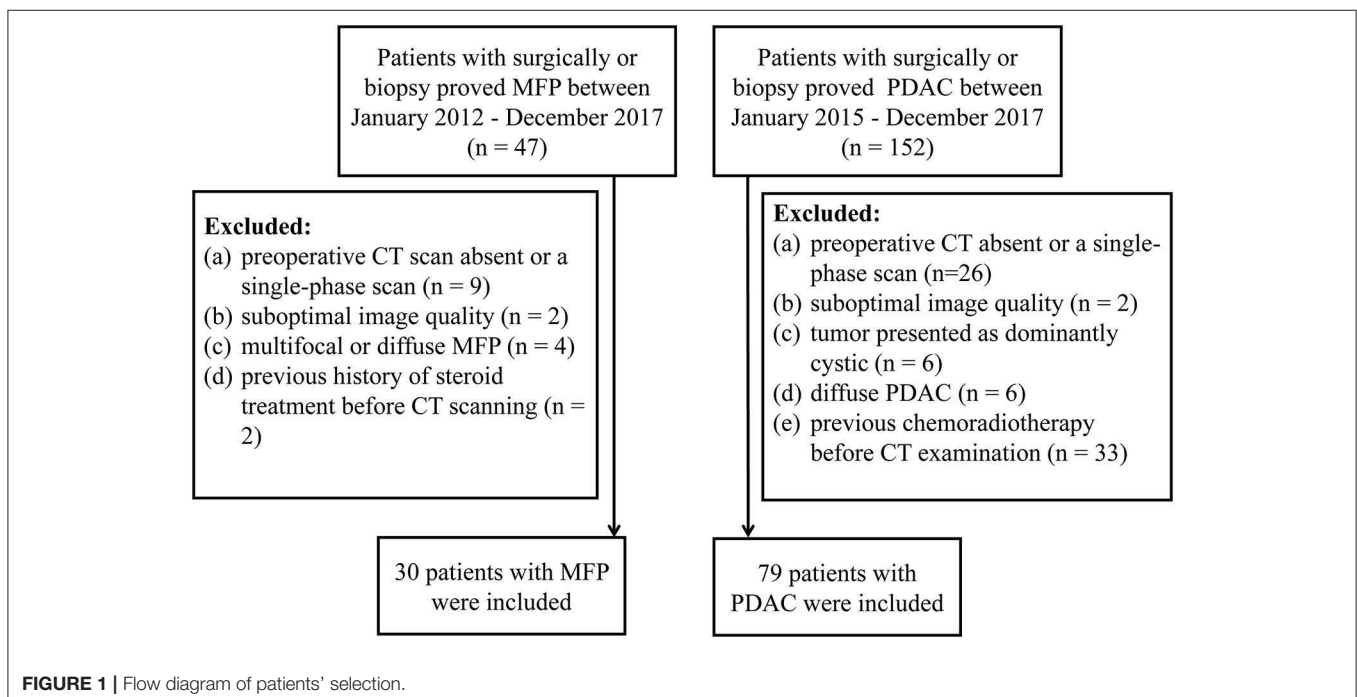
Several previous studies have proved that dual-energy CT, perfusion CT, and diffusion-weighted magnetic resonance imaging can be utilized for discriminating MFP from PDAC (7–10, 13, 18). With the application of extracting, analyzing, and interpreting quantitative imaging features, texture analysis has recently been applied to cancer diagnosis, treatment response, and prognosis evaluation (19). However, no studies have investigated the potential of texture analysis in differential diagnosis between the two lesions. The aim of our study was to investigate the diagnostic performance of CT imaging features and texture analysis in the differentiation between the two lesions.

MATERIALS AND METHODS

Patient data confidentiality was protected in accordance with the Declaration of Helsinki principles. The protocol was approved by the institutional review board of the Affiliated Hospital of Nanjing University of Chinese Medicine. Written informed consent was waived because it is a retrospective study.

Patient Selection

From January 2012 to December 2017, 47 consecutive patients with surgically- ($n = 29$) or biopsy- ($n = 18$) proved MFP were identified from our medical records. Inclusion criteria were: (1) contrast-enhanced CT performed <30 days prior to resection or biopsy; (2) clinical characteristics available. The exclusion



criteria were: (1) preoperative CT scan absent or only single-phase obtained ($n = 9$); or (2) suboptimal image quality ($n = 2$); (3) multifocal or diffuse MFP ($n = 4$); (4) history of steroid treatment before CT scan ($n = 2$). Ultimately, a total of 30 patients (25 males and 5 females; mean age 61.47 ± 12.43 years; age range 43–74 years) were included in our study (Figure 1).

Similarly, from January 2015 to December 2017, 152 consecutive patients with surgically- ($n = 130$) or biopsy- ($n = 22$) proved PDAC were identified from our medical records. Inclusion criteria were: (1) contrast-enhanced CT performed <30 days prior to resection or biopsy; (2) clinical characteristics available. The exclusion criteria were: (1) preoperative CT scan absent or only single-phase scan obtained ($n = 26$); or (2) suboptimal image quality ($n = 2$); or (3) tumor presented as dominantly cystic ($n = 6$); (4) diffuse PDAC ($n = 6$); (5) previous chemoradiotherapy before CT examination ($n = 33$). Ultimately, a total of 79 patients (56 males and 23 females; mean age 65.18 ± 8.60 years; age range, 61–84 years) were included in our study (Figure 1).

CT Imaging

Multi-detector CT systems, including Philips Brilliance 64 (Philips Healthcare, DA Best, the Netherlands) and Optima 670

(GE Healthcare, Tokyo, Japan), were used for CT scanning following a standardized protocol. Three-phase examinations consisted of unenhanced, arterial, and portal phases were performed on all patients. CT scanning parameters were as follows: tube voltage, 120 kVp; current, 200–400 mAs; pitch, 1.375; rotation speed, 0.75 s; slice thickness, 3.0 mm; slice interval, 3.0 mm; and a reconstruction interval of 1.25 mm. Following unenhanced imaging, non-ionic contrast media Ultravist 300 (Bayer Schering Pharma AG, Berlin, Germany) was administered intravenously (1.2–1.5 ml/kg) at a rate of 3.0 ml/s followed by 40 ml saline solution, using a power injector (Ulrich Medical, Ulm, Germany). Arterial and portal phase scanning were obtained at 35 and 60 s.

Image Analysis

CT images were evaluated by two independent blinded abdominal radiologists (SR and JZ). Disparities in image analysis were resolved by discussion with a senior radiologist (JC) until consensus was reached. The following imaging features were evaluated: tumor location, shape, margin, cystic degeneration, calcification, enhancement pattern, degree and shape of pancreatic ductal dilatation, pancreatic duct penetrating sign, vascular invasion, pancreatic sinistral portal hypertension,

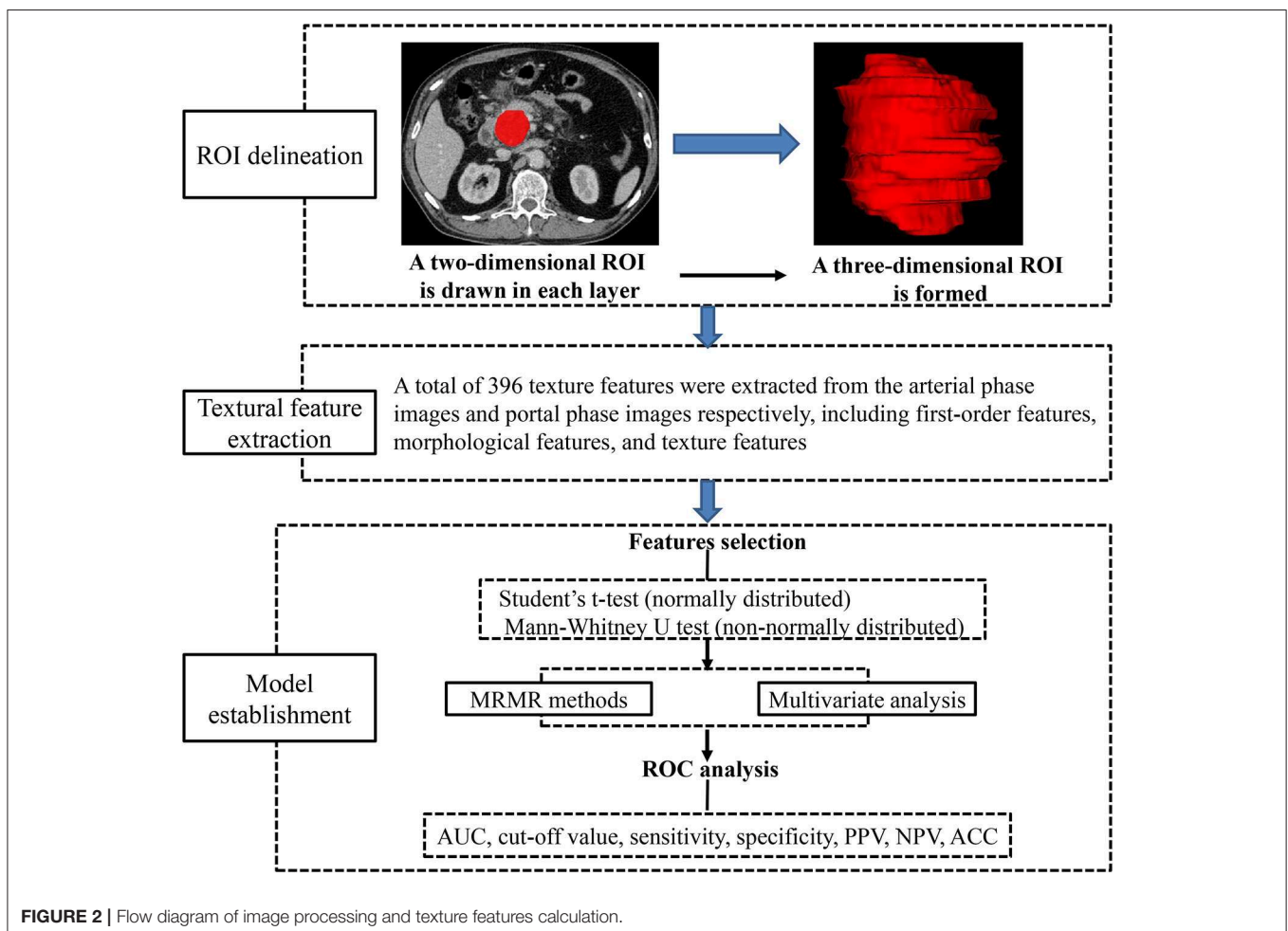


TABLE 1 | Clinical data of patients with MFP and PDAC.

Variables	MFP (n = 30)	PDAC (n = 79)	P-value
Age (years)	61.47 ± 12.43	65.18 ± 8.60	0.140
Gender			0.184
Male	25 (83.33%)	56 (70.89%)	
Female	5 (16.67%)	23 (29.11%)	
Clinical symptoms			
A history of pancreatitis	19 (73.1%)	12 (14.6%)	< 0.001
Abdominal pain	25 (83.33%)	62 (78.48%)	0.573
Yellow urine or icterus	8 (26.67%)	27 (34.18%)	0.453
Nausea and vomiting	5 (16.67%)	11 (13.92%)	0.953
Weight loss	2 (6.67%)	13 (16.46%)	0.311
Fever	3 (10.00%)	2 (2.53%)	0.249

TABLE 2 | CT imaging features of patients with MFP and PDAC.

CT findings	MFP (n = 30)	PDAC (n = 79)	p-value
Location			0.150
Head and neck	24 (80%)	52 (65.8%)	
Body and tail	6 (20%)	27 (34.2%)	
Shape (oval/lobulation/irregular)	20/3/7	62/5/12	0.443
Margin			0.707
Well-defined	2 (6.7%)	9 (11.4%)	
Ill-defined	28 (93.3%)	70 (88.6%)	
Cystic degeneration	8 (25.8%)	37 (46.8%)	0.044
Calcification	6 (20%)	6 (7.6%)	0.065
Enhancement pattern			0.140
Homogeneous	21 (70%)	43 (54.4%)	
Heterogeneous	9 (30%)	36 (45.6%)	
Pancreatic duct dilatation	11 (36.7%)	47 (59.5%)	0.033
Degree (low to moderate/severe)	9/2	34/13	0.792
Shape (Uniformity/Beaded expansion)	4/7	39/8	0.005
Pancreatic duct penetrating sign	20 (66.7%)	15 (19%)	<0.001
Vascular invasion	5 (16.7%)	42 (53.2%)	0.001
Pancreatic sinistral portal hypertension	4 (13.3%)	31 (39.2%)	0.010
Peripancreatic exudation	11 (36.7%)	18 (22.8%)	0.143
Lymph nodes enlargement	12 (40.0%)	42 (53.2%)	0.220
Size (cm)	4.05 ± 1.02	3.41 ± 1.16	0.009
Arterial CT attenuation (HU)	60.57 ± 11.24	51.82 ± 11.36	<0.001
Portal CT attenuation (HU)	75.17 ± 11.04	71.53 ± 13.94	0.203
Arterial enhancement ratio	0.89 ± 0.20	0.66 ± 0.15	<0.001
Portal enhancement ratio	0.89 ± 0.19	0.77 ± 0.17	0.004

HU, Hounsfield unit.

peripancreatic exudation, and lymph nodes enlargement. A smooth and clearly visible margin was considered to be well-defined, while spiculation or infiltration on >90° of tumor perimeter was considered to be ill-defined (20). Tumor thrombus, vessel occlusion, stenosis or contour deformity indicated vascular invasion (21). An enhancing solid portion of <50% of the tumor was regarded as cystic degeneration (22). Unenhanced images was used to identify calcifications. The senior radiologist (JC) measured size (cm) and CT attenuation

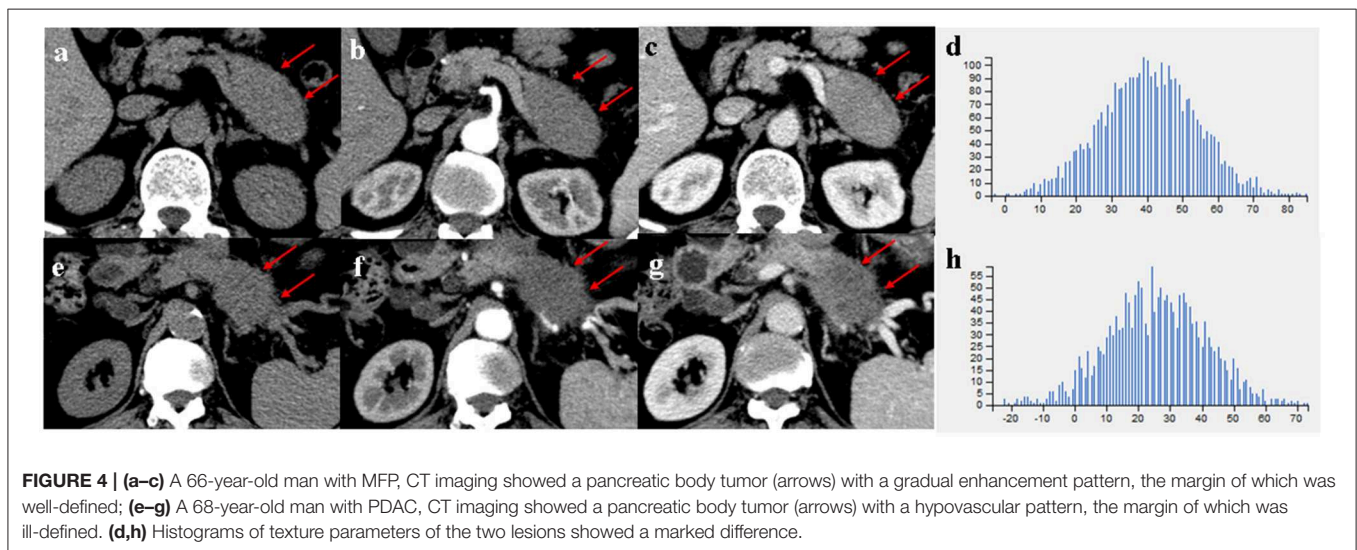
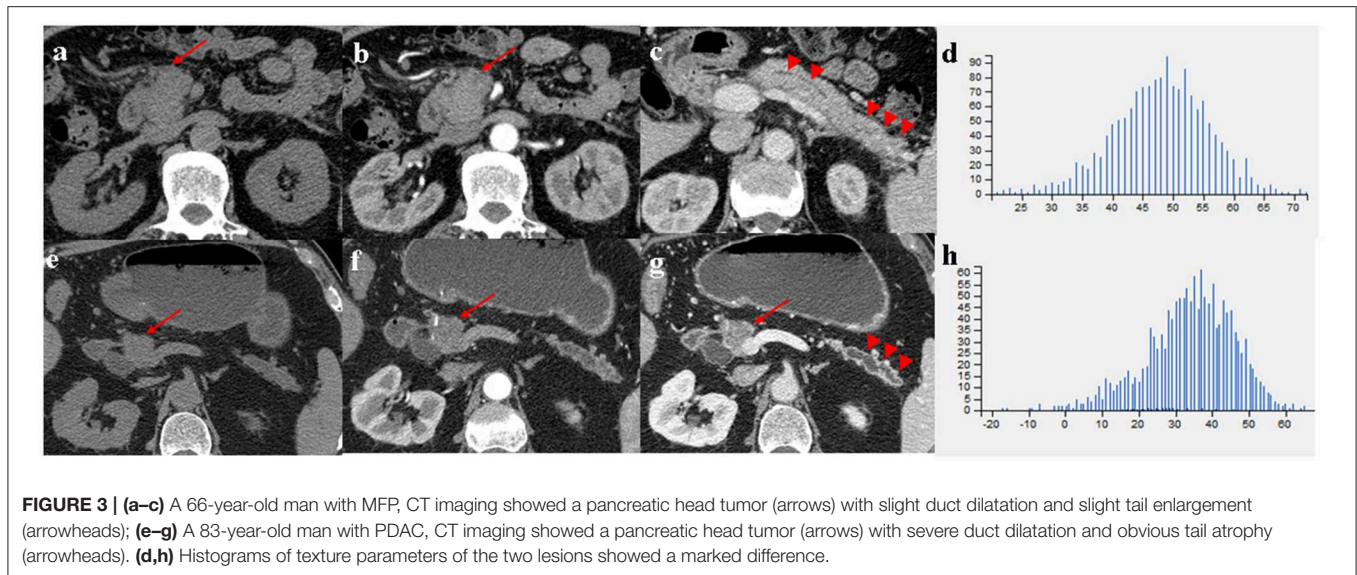
(HU) of lesions and adjacent parenchyma three times with region of interest (ROI) delineating. ROIs encompassed the solid components, avoiding intratumoral calcification, and cystic degeneration. Arterial and portal enhancement ratios were calculated by dividing CT attenuation (HU) of the tumor by that of the pancreatic parenchyma in arterial and portal phases, respectively (17).

Texture Analysis

Preoperative images obtained in arterial and portal phases were exported in DICOM format from medical database to ITK-SNAP for ROI delineation. ROIs were manually drawn along the margin of the tumor in every visualized tumor image in consensus by two radiologists (SR and JC), avoiding peripheral fat, artifacts, and blood vessels in order to eliminate non-tumor tissue effect. All DICOM images and their corresponding ROIs were individually transferred to AnalysisKit software (Version V3.0.0.R, GE Healthcare) for texture features extraction. Image processing and texture feature analysis are demonstrated in **Figure 2**. As referring to Image Biomarker Standardization Initiative (ISBI), three categories of radiomic features were calculated. (1) first-order features, which describe the distribution of voxel intensities within the ROI. (2) Morphological features, which describe geometric aspects of a ROI, such as area and volume. (3) Texture features, which describe high-order gray information within the ROI, they are calculated based on three matrices, the gray-level co-occurrence matrix (GLCM), a matrix that expresses how combinations of discretized gray levels of neighboring pixels, or voxels in a 3D volume, are distributed along one of the image directions, the run length matrix (RLM), assesses the length of a consecutive sequence of pixels or voxels with the same gray level along one direction, the gray level size zone matrix (GLSZM), counts the number of groups (or zones) of linked voxels. A total of 396 texture features were extracted from each image in our study.

Statistical Analysis

Statistical analysis was performed with R software, version 3.5.3 (<https://www.r-project.org>). Conventional contrast-enhanced CT imaging features were compared between MFP and PDAC using Chi-square or Fisher's exact test for categorical variables and the Student's *t*-test or Mann-Whitney *U*-test for continuous variables. Minimum redundancy maximum relevance (MRMR) was performed for radiomic feature selection to reduce the redundancy and unnecessary complexity of the computation and modeling (23). A stepwise-backward multivariate logistic regression was used to identify relevant CT imaging and texture features and construct radiomic models to discriminate MFP from PDAC. Receiver operating characteristic (ROC) curve analysis was used to validate the performance of predicting models by providing area under the curve (AUC), sensitivity, specificity, accuracy, positive predictive value (PPV) and negative predictive value (NPV). *P* < 0.05 was considered statistically significant.



RESULTS

Patients' Clinical Characteristics

The clinical characteristics of 30 MFP and 79 PDAC patients are summarized in **Table 1**. No significant differences were found in age, sex or clinical symptoms between the two groups with the exception of a history of pancreatitis, which was more common in MFP than PDAC (73.1 vs. 14.6%, $p < 0.001$).

Comparison of CT Imaging Features Between MFP and PDAC

Comparison of CT imaging features between MFP and PDAC is summarized in **Table 2**. No statistically significant differences with respect to tumor location, shape, margin, calcification, peripancreatic exudation, or lymph nodes enlargement were observed between MFP and PDAC patients. Pancreatic ductal dilatation was more frequent in PDAC than MFP [59.5% (47 of

79) vs. 36.7% (11 of 30), $p = 0.033$]. However, no statistically significant difference with respect to degree of pancreatic ductal dilatation was observed between the two groups. In those lesions with duct dilatation, uniformity of dilatation was more common in PDAC than MFP [83.0% (39 of 47) vs. 36.4% (4 of 11)] and beaded dilatation was more common in MFP than PDAC [63.6% (7 of 11) vs. 17.0% (8 of 47)] with a p -value of 0.005. Pancreatic duct penetrating sign was more common in MFP compared to PDAC [66.7% (20 of 30) vs. 19.0% (15 of 79), $p < 0.001$]. Moreover, cystic degeneration, vascular invasion, and pancreatic sinistral portal hypertension were more frequent in PDAC than MFP (all $p < 0.05$). Cystic degeneration was found in 46.8% (37/79) of PDAC, vascular invasion was found in 53.2% (42/79) of PDAC, and pancreatic sinistral portal hypertension was found in 39.2% (31/79) of PDAC, while only 25.8% (8/30), 16.7% (5/30), and 13.3% (4/30), respectively, of MFP exhibited such imaging features. **Figures 3, 4** show representative cases

of MFP (Figures 3a–c, 4a–c) and PDAC (Figures 3e–g, 4e–g) tumors located at pancreatic head and body, respectively.

Tumor size was larger in MFP than PDAC ($4.05 \text{ cm} \pm 1.02$ vs. $3.41 \text{ cm} \pm 1.16$, $p = 0.009$). Arterial CT attenuation of MFP was significantly higher than PDAC ($59.24 \pm 13.11 \text{ HU}$ vs. $44.36 \pm 8.66 \text{ HU}$, $p < 0.001$), while no significant difference was observed between MFP and PDAC with respect to unenhanced or portal CT attenuation ($p > 0.05$; Figure 5). Arterial and portal enhancement ratios of MFP were significantly higher than PDAC ($p < 0.001$, $p = 0.004$; Figure 6).

Multivariate logistic regression was performed to ascertain relevant CT imaging features in differentiating the two lesions. Arterial CT attenuation and pancreatic duct penetrating sign were independent predictors of CT imaging features

in differentiating the two lesions (Table 3). The diagnostic performance of each imaging feature is demonstrated in Supplementary Table 1. ROC curve was adopted to determine the diagnostic performance of imaging feature-based model (Model 1) in differentiating MFP from PDAC (Figure 7). Parameters of Model 1 including AUC, cut-off value, diagnostic sensitivity (%), specificity (%), accuracy (%), PPV (%), and NPV (%) were 0.84, 0.787, 77, 86, 72, 91, and 57%, respectively (Table 4).

Comparison of CT Texture Analysis Between MFP and PDAC

A total of 396 texture features were extracted from each image in arterial or portal phase. Multivariate logistic

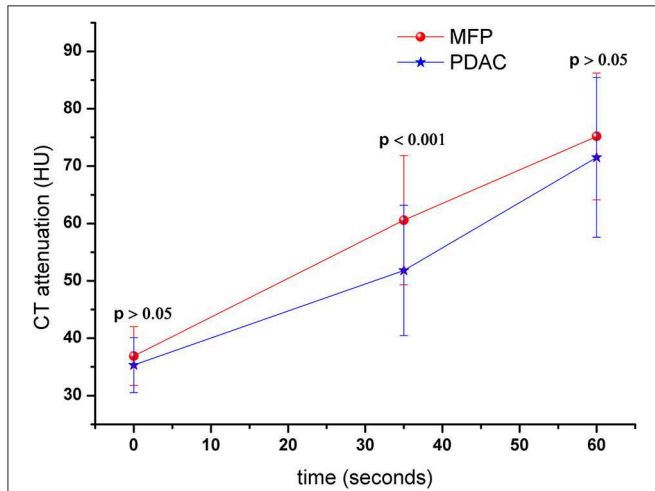


FIGURE 5 | Dynamic contrast-enhanced curves of patients with MFP and PDAC. CT attenuation of MFP and PDAC was 41.52 ± 5.79 and 42.00 ± 5.37 Hounsfield units in unenhanced phase, respectively. CT attenuation of MFP was higher than PDAC in arterial phase ($p < 0.001$).

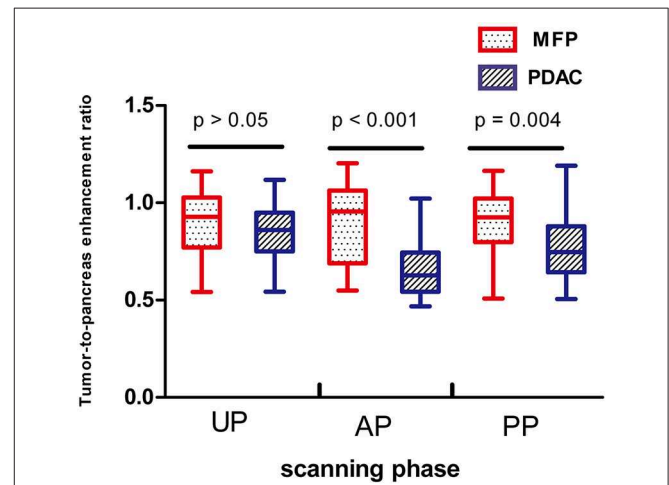
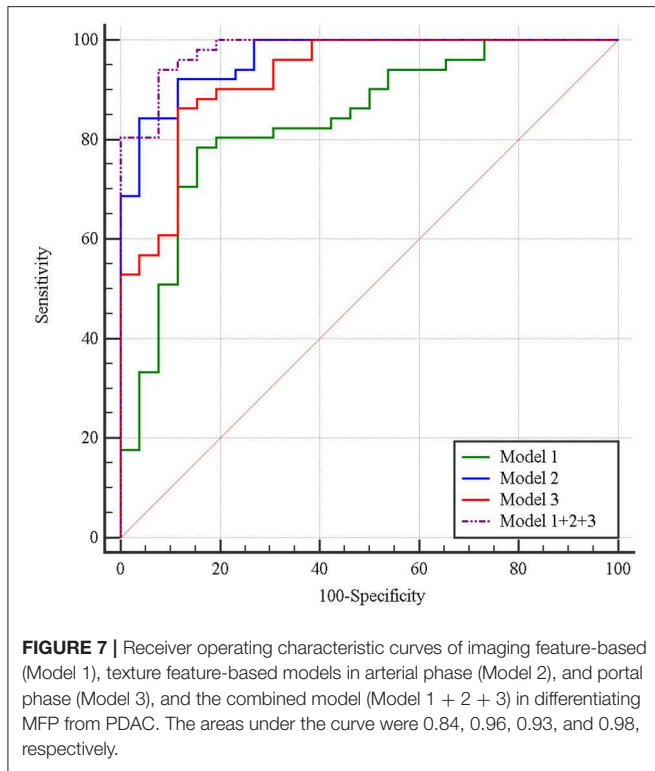


FIGURE 6 | Box-and-whisker plots of enhancement ratios of patients with MFP and PDAC in unenhanced, arterial, and portal phases. Enhancement ratios of MFP were higher than PDAC in arterial phase (AP, $p < 0.001$) and portal phase (PP, $p = 0.004$).

TABLE 3 | Multivariate analyses of CT imaging and texture parameters in differentiating MFP from PDAC.

	Characteristics	OR	95% (CI)	P-value
CT features	Arterial CT attenuation	0.943	0.911–0.976	0.001
	Pancreatic duct penetrating sign	0.119	0.043–0.333	<0.001
Texture features	AP			
	Surface Area	0.282	0.095–0.672	0.008
	Percentile40	0.042	0.005–0.201	<0.001
	InverseDifferenceMoment_angle90_offset4	0.129	0.024–0.486	0.006
	LongRunEmphasis_angle45_offset4	0.326	0.095–0.868	0.041
	uniformity	6.722	1.124–40.268	0.029
PP	LongRunEmphasis_angle135_offset7	0.394	0.104–1.274	0.060
	VoxelValueSum	0.253	0.097–0.546	0.001
	LongRunEmphasis_angle135_offset4	0.529	0.209–1.244	0.069
	GLCMEntropy_angle45_offset1	2.169	0.946–6.773	0.007

OR, odds ratio; CI, confidence interval; AP, arterial phase; PP, portal phase.



regression was performed to ascertain relevant CT texture features in differentiating the two lesions. SurfaceArea, Percentile40, InverseDifferenceMoment_angle90_offset4, LongRunEmphasis_angle45_offset4, and uniformity were independent predictors of arterial texture parameters in differentiating the two lesions (Table 3). LongRunEmphasis_angle135_offset7, VoxelValueSum, LongRunEmphasis_angle135_offset4, and GLCMEntropy_angle45_offset1 were independent predictors of portal texture parameters in differentiating the two lesions (Table 3). The diagnostic performance of each texture feature in arterial and portal phases is shown in Supplementary Table 1. ROC curves were adopted to determine the diagnostic performance of arterial texture feature-based model (Model 2) and portal texture feature-based model (Model 3) in differentiating MFP from PDAC (Figure 7). Parameters of Model 2 including AUC, cut-off value, sensitivity (%), specificity (%), accuracy (%), PPV (%), and NPV (%) were 0.96, 1.502, 96, 83, 87, 74, and 98%, respectively (Table 4). Parameters of Model 3 including AUC, cut-off value, diagnostic sensitivity (%), specificity (%), accuracy (%), PPV (%), and NPV (%) were 0.93, 0.347, 77, 94, 89, 87, and 89%, respectively (Table 4).

Subsequently, the diagnostic ability of the combined model based on imaging features and texture features (Model 1 + 2 + 3) was also evaluated via ROC curve analysis (Figure 7). The AUC was 0.98 with 94% sensitivity, 92% specificity, 94% accuracy, 96% PPV, and 89% NPV for discriminating MFP from PDAC (Table 4).

Finally, we randomly selected 40 samples for internal validation, including 10 MFP (33.3%), and 30 PDAC tumors

TABLE 4 | Diagnostic performance of imaging feature-based (Model 1), texture feature-based models in arterial phase (Model 2), and portal phase (Model 3), and the combined model (Model 1 + 2 + 3) for differentiating MFP from PDAC.

Model	AUC (95% CI)	Cut-off value (SEN%, SPE%)	PPV (%)	NPV (%)	ACC (%)
Model 1	0.84 (0.75–0.92)	0.787 (77, 86)	91	57	72
Model 2	0.96 (0.93–1.0)	1.502 (96, 83)	74	98	87
Model 3	0.93 (0.87–0.98)	0.347 (77, 94)	87	89	89
Model 1 + 2 + 3	0.98 (0.92–1.0)	0.598 (94, 92)	96	89	94

AUC, area under the curve; SEN, sensitivity; SPE, specificity; PPV, positive predictive value; NPV, negative predictive value; CI, confidence interval.

(38.0%). The AUCs of texture feature-based models in arterial and portal phases were 0.90 (90% sensitivity, 81% specificity, 64% PPV, 96% NPV, and 75% accuracy) and 0.87 (66% sensitivity, 96% specificity, 52% PPV, 98% NPV, and 74% accuracy), respectively. The verification results are similar to previous studies, which prove that the model is comparatively reproducible and stable.

DISCUSSION

Chronic pancreatitis and PDAC are commonly seen in clinical practice, but only a small portion of chronic pancreatitis presents as MFP. The overlap in clinical and radiologic features of the two lesions makes their early preoperative differential diagnosis difficult (7–11, 24–26). Misdiagnosis of MFP as PDAC may result in unnecessary interventional procedures, and misdiagnosis of PDAC as MFP may result in delayed surgical treatment (10). In the present study, we evaluated the role of CT imaging and texture analysis in differentiating MFP from PDAC. Our data indicate that CT texture analysis demonstrates great potential in differentiating MFP from PDAC.

Treatment strategies and management are geared to pancreatic tumor type. Early preoperative differentiation between MFP and PDAC would be especially useful for treatment planning. Although a fine-needle biopsy is an accurate method in tumor identification, imaging plays a crucial role in estimating the aggressiveness of the tumor and facilitating in treatment approaches planning. Previous CT or MRI studies indicate that internal cystic or necrotic portion, peripancreatic fat infiltration, vascular invasion, uniformity of pancreatic duct expansion, and lymph nodes enlargement are more frequent in PDAC, while beaded pancreatic duct expansion and duct penetrating sign are more frequent in MFP (10, 18, 24). Our data is in consistent with the findings, and in addition we found that pancreatic sinistral portal hypertension was more common in PDAC than MFP. We also evaluated the value of CT attenuation and enhancement ratio in differentiating MFP from PDAC. We found that arterial CT attenuation, arterial and portal enhancement ratios were significantly higher in MFP than PDAC. In multivariate analyses, arterial CT attenuation and pancreatic duct penetrating sign were independent predictors in differentiating MFP from PDAC.

CT and MRI imaging findings provide mostly qualitative evaluation. The use of quantitative parameters could enhance

diagnosis. Texture analysis is an emerging imaging-based post-processing method that allows for quantification of tissue heterogeneity (27). There has been a surge in recent years in the research application of CT texture analysis in tumor identification, staging, and therapy response assessment (19, 23, 27, 28). However, no studies have demonstrated the value of CT texture analysis in differentiating MFP from PDAC. We are the first to use CT texture analysis to differentiate MFP from PDAC. Our data show that SurfaceArea, Percentile40, InverseDifferenceMoment_angle90_offset4, LongRunEmphasis_angle45_offset4, and uniformity on arterial phase images and LongRunEmphasis_angle135_offset7, VoxelValueSum, LongRunEmphasis_angle135_offset4, and GLCMEntropy_angle45_offset1 on portal phase images are independent predictors in discriminating MFP from PDAC. Moreover, our data indicate that CT imaging features can obtain good specificity but poor sensitivity in differentiating the two lesions. However, texture analyses in arterial phase can obtain high pooled sensitivity and specificity. The combined model based on imaging features and texture features reveal high pooled sensitivity of 94%, specificity of 92%, accuracy of 94, 96% PPV, and 89% NPV. Texture analyses can effectively improve the efficacy of contrast-enhanced CT for differentiating MFP from PDAC.

We acknowledge the following limitations of our study. First, only patients with pathologically proved MFP or PDAC were included in our study, which may result in a selection bias due to the lower incidence of MFP than PDAC. However, this step is an essential inclusion criterion for the aim of validating the correlation between CT texture analyses and tumor types. Second, inter-observer variability for tumor segmentation could not be obtained due to the consensus review by radiologists. Third, the enrolled number of patients is relatively small for CT texture analysis. There are two main reasons for the relatively small sample size: (1) MFP is a special type of chronic pancreatitis, which accounts for 10–30% of chronic pancreatitis (11). It is relatively difficult to collect enough patients in a short time period. (2) To meet the requirement of high consistency of scanning equipment and parameter and to guarantee the accuracy of texture analysis (29), some cases should be excluded from the cohort. But since the enrolled patients were not sufficient, all cases were included, and an internal validation was

adopted to verify the results in order to guarantee the accuracy of the test set as best as the existing conditions permit. A multicenter program to include more MFP patients may be needed, and an external validation to confirm the potential value of CT texture analyses in discriminating MFP from PDAC may also be needed.

In conclusion, we found that multiple CT imaging and texture parameters are significantly different between MFP and PDAC groups. Larger-cohort studies, preferably multicenter, to confirm the potential value of CT texture analyses in differentiating MFP from PDAC are in order.

DATA AVAILABILITY STATEMENT

All datasets generated for this study are included in the article/**Supplementary Material**.

AUTHOR CONTRIBUTIONS

SR, XC, and ZW designed the study. JZ, JC, WC, WQ, and RZ conducted the experiments. JC, SD, and RC analyzed the data. SR wrote the draft. All authors read and approved the final manuscript.

FUNDING

This study was funded by Jiangsu Provincial Key Research and Development Program (BE2017772), Administration of Traditional Chinese Medicine of Jiangsu Province (ZD201907), and the National Natural Science Foundation of China (81771899).

ACKNOWLEDGMENTS

Thanks to the continuous and excellent support of all authors and colleagues.

SUPPLEMENTARY MATERIAL

The Supplementary Material for this article can be found online at: <https://www.frontiersin.org/articles/10.3389/fonc.2019.01171/full#supplementary-material>

REFERENCES

- Zou X, Wei J, Huang Z, Zhou X, Lu Z, Zhu W, et al. Identification of a six-miRNA panel in serum benefiting pancreatic cancer diagnosis. *Cancer Med*. (2019) 8:2810–22. doi: 10.1002/cam4.2145
- Xu Y, Hannafon BN, Zhao YD, Postier RG, Ding WQ. Plasma exosome miR-196a and miR-1246 are potential indicators of localized pancreatic cancer. *Oncotarget*. (2017) 8:77028–40. doi: 10.18632/oncotarget.20332
- Zhou B, Xu JW, Cheng YG, Gao JY, Hu SY, Wang L, et al. Early detection of pancreatic cancer: Where are we now and where are we going? *Int J Cancer*. (2017) 141:231–41. doi: 10.1002/ijc.30670
- Knudsen ES, O'Reilly EM, Brody JR, Witkiewicz AK. Genetic diversity of pancreatic ductal adenocarcinoma and opportunities for precision medicine. *Gastroenterology*. (2016) 150:48–63. doi: 10.1053/j.gastro.2015.08.056
- Matsubayashi H, Matsui T, Yabuuchi Y, Imai K, Tanaka M, Kakushima N, et al. Endoscopic ultrasonography guided-fine needle aspiration for the diagnosis of solid pancreaticobiliary lesions: clinical aspects to improve the diagnosis. *World J Gastroenterol*. (2016) 22:628–40. doi: 10.3748/wjg.v22.i2.628
- Lee H, Lee JK, Kang SS, Choi D, Jang KT, Kim JH, et al. Is there any clinical or radiologic feature as a preoperative marker for differentiating mass-forming pancreatitis from early-stage pancreatic adenocarcinoma? *Hepatogastroenterology*. (2007) 54:2134–40.
- Yin Q, Zou X, Zai X, Wu Z, Wu Q, Jiang X, et al. Pancreatic ductal adenocarcinoma and chronic mass-forming pancreatitis: differentiation with dual-energy MDCT in spectral imaging mode. *Eur J Radiol*. (2015) 84:2470–6. doi: 10.1016/j.ejrad.2015.09.023
- Aslan S, Nural MS, Camlidag I, Danaci M. Efficacy of perfusion CT in differentiating of pancreatic ductal adenocarcinoma from mass-forming

- chronic pancreatitis and characterization of isoattenuating pancreatic lesions. *Abdom Radiol.* (2019) 44:593–603. doi: 10.1007/s00261-018-1776-9
9. Yadav AK, Sharma R, Kandasamy D, Pradhan RK, Garg PK, Bhalla AS, et al. Perfusion CT – Can it resolve the pancreatic carcinoma versus mass forming chronic pancreatitis conundrum? *Pancreatol.* (2016) 16:979–87. doi: 10.1016/j.pan.2016.08.011
 10. Ruan Z, Jiao J, Min D, Qu J, Li J, Chen J, et al. Multi-modality imaging features distinguish pancreatic carcinoma from mass-forming chronic pancreatitis of the pancreatic head. *Oncol Lett.* (2018) 15:9735–44. doi: 10.3892/ol.2018.8545
 11. Gu X, Liu R. Application of 18F-FDG PET/CT combined with carbohydrate antigen 19-9 for differentiating pancreatic carcinoma from chronic mass-forming pancreatitis in Chinese elderly. *Clin Interv Aging.* (2016) 11:1365–70. doi: 10.2147/CIA.S115254
 12. Balthazar EJ. Pancreatitis associated with pancreatic carcinoma. Preoperative diagnosis: role of CT imaging in detection and evaluation. *Pancreatol.* (2005) 5:330–44. doi: 10.1159/000086868
 13. Sandrasegaran K, Nutakki K, Tahir B, Dhanabal A, Tann M, Cote GA. Use of diffusion-weighted MRI to differentiate chronic pancreatitis from pancreatic cancer. *Am J Roentgenol.* (2013) 201:1002–8. doi: 10.2214/AJR.12.10170
 14. Birgin E, Hablawetz P, Téoule P, Rückert F, Wilhelm TJ. Chronic pancreatitis and resectable synchronous pancreatic carcinoma : a survival analysis. *Pancreatol.* (2018) 18:394–8. doi: 10.1016/j.pan.2018.04.009
 15. Kirkegård J, Mortensen FV, Cronin-Fenton D. Chronic pancreatitis and pancreatic cancer risk: a systematic review and meta-analysis. *Am J Gastroenterol.* (2017) 112:1366–72. doi: 10.1038/ajg.2017.218
 16. Facciorusso A, Wani S, Triantafyllou K, Tziatzios G, Cannizzaro R, Muscatiello N, et al. Comparative accuracy of needle sizes and designs for EUS tissue sampling of solid pancreatic masses: a network meta-analysis. *Gastrointest Endosc.* (2019). doi: 10.1016/j.gie.2019.07.009. [Epub ahead of print].
 17. Zhang B, Zhu F, Li P, Yu S, Zhao Y, Li M. Endoscopic ultrasound elastography in the diagnosis of pancreatic masses: a meta-analysis. *Pancreatol.* (2018) 18:833–40. doi: 10.1016/j.pan.2018.07.008
 18. Choi SY, Kim SH, Kang TW, Song KD, Park HJ, Choi YH. Differentiating mass-forming autoimmune pancreatitis from pancreatic ductal adenocarcinoma on the basis of contrast-enhanced MRI and DWI findings. *Am J Roentgenol.* (2016) 206:291–300. doi: 10.2214/AJR.15.14974
 19. Lubner MG, Smith AD, Sandrasegaran K, Sahani DV, Pickhardt PJ. CT texture analysis: definitions, applications, biologic correlates, and challenges. *Radiographics.* (2017) 37:1483–503. doi: 10.1148/rg.2017170056
 20. Ren S, Chen X, Wang Z, Zhao R, Wang J, Cui W, et al. Differentiation of hypovascular pancreatic neuroendocrine tumors from pancreatic ductal adenocarcinoma using contrast-enhanced computed tomography. *PLoS ONE.* (2019) 14:e0211566. doi: 10.1371/journal.pone.0211566
 21. Kim DW, Kim HJ, Kim KW, Byun JH, Song KB, Kim JH, et al. Neuroendocrine neoplasms of the pancreas at dynamic enhanced CT: comparison between grade 3 neuroendocrine carcinoma and grade 1/2 neuroendocrine tumour. *Eur Radiol.* (2015) 25:1375–83. doi: 10.1007/s00330-014-3532-z
 22. Jeon SK, Lee JM, Joo I, Lee ES, Park HJ, Jang JY, et al. Nonhypervascular pancreatic neuroendocrine tumors: differential diagnosis from pancreatic ductal adenocarcinomas at MR imaging-retrospective cross-sectional study. *Radiology.* (2017) 284:77–87. doi: 10.1148/radiol.2016160586
 23. Gu D, Hu Y, Ding H, Wei J, Chen K, Liu H, et al. CT radiomics may predict the grade of pancreatic neuroendocrine tumors: a multicenter study. *Eur Radiol.* (2019). doi: 10.1007/s00330-019-06176-x. [Epub ahead of print].
 24. Muhi A, Ichikawa T, Motosugi U, Sou H, Sano K, Tsukamoto T, et al. Mass-forming autoimmune pancreatitis and pancreatic carcinoma: differential diagnosis on the basis of computed tomography and magnetic resonance cholangiopancreatography, and diffusion-weighted imaging findings. *J Magn Reson Imaging.* (2012) 35:827–36. doi: 10.1002/jmri.22881
 25. Klau M, Lemke A, Grünberg K, Simon D, Re TJ, Wente MN, et al. Intravoxel incoherent motion MRI for the differentiation between mass forming chronic pancreatitis and pancreatic carcinoma. *Invest Radiol.* (2011) 46:57–63. doi: 10.1097/RLI.0b013e3181fb3bf2
 26. Dutta AK, Chacko A. Head mass in chronic pancreatitis: inflammatory or malignant. *World J Gastrointest Endosc.* (2015) 7:258–64. doi: 10.4253/wjge.v7.i3.258
 27. Cannella R, Borhani AA, Minervini MI, Tsung A, Furlan A. Evaluation of texture analysis for the differential diagnosis of focal nodular hyperplasia from hepatocellular adenoma on contrast-enhanced CT images. *Abdom Radiol.* (2019) 44:1323–30. doi: 10.1007/s00261-018-1788-5
 28. Guo C, Zhuge X, Wang Q, Xiao W, Wang Z, Wang Z, et al. The differentiation of pancreatic neuroendocrine carcinoma from pancreatic ductal adenocarcinoma: the values of CT imaging features and texture analysis. *Cancer Imaging.* (2018) 18:37. doi: 10.1186/s40644-018-0170-8
 29. Cui WJ, Wang C, Jia L, Ren S, Duan SF, Cui C, et al. Differentiation between G1 and G2/G3 phyllodes tumors of breast using mammography and mammographic texture analysis. *Front Oncol.* (2019) 9:433. doi: 10.3389/fonc.2019.00433

Conflict of Interest: SD was employed by the company GE healthcare.

The remaining authors declare that the research was conducted in the absence of any commercial or financial relationships that could be construed as a potential conflict of interest.

Copyright © 2019 Ren, Zhang, Chen, Cui, Zhao, Qiu, Duan, Chen, Chen and Wang. This is an open-access article distributed under the terms of the Creative Commons Attribution License (CC BY). The use, distribution or reproduction in other forums is permitted, provided the original author(s) and the copyright owner(s) are credited and that the original publication in this journal is cited, in accordance with accepted academic practice. No use, distribution or reproduction is permitted which does not comply with these terms.